Src kinase activation: A switched electrostatic network

Elif Ozkirimli and Carol Beth Post

Protein Sci. 2006 15: 1051-1062; originally published online Apr 5, 2006;
doi:10.1110/ps.051999206

Src kinase activation: A switched electrostatic network

ELIF OZKIRIMLI AND CAROL BETH POST

Medicinal Chemistry and Molecular Pharmacology Department, Markey Center for Structural Biology and Purdue Cancer Center, Purdue University, West Lafayette, Indiana 47907-2091, USA

(RECEIVED November 28, 2005; FINAL REVISION January 28, 2006; ACCEPTED January 31, 2006)

Abstract

Src tyrosine kinases are essential in numerous cell signaling pathways, and improper functioning of these enzymes has been implicated in many diseases. The activity of Src kinases is regulated by conformational activation, which involves several structural changes within the catalytic domain (CD): the orientation of two lobes of CD; rearrangement of the activation loop (A-loop); and movement of an α-helix (αC), which is located at the interface between the two lobes, into or away from the catalytic cleft. Conformational activation was investigated using biased molecular dynamics to explore the transition pathway between the active and the down-regulated conformation of CD for the Src-kinase family member Lyn kinase, and to gain insight into the interdependence of these changes. Lobe opening is observed to be a facile motion, whereas movement of the A-loop motion is more complex requiring secondary structure changes as well as communication with αC. A key result is that the conformational transition involves a switch in an electrostatic network of six polar residues between the active and the down-regulated conformations. The exchange between interactions links the three main motions of the CD. Kinetic experiments that would demonstrate the contribution of the switched electrostatic network to the enzyme mechanism are proposed. Possible implications for regulation conferred by interdomain interactions are also discussed.

Keywords: enzyme activation; protein electrostatics; activated molecular dynamics; allosterism; phosphoproteins

The Src tyrosine kinase family plays an essential role in numerous pathways of cellular signaling (Bolen and Brugge 1997; Thomas and Brugge 1997). Part of the regulatory mechanism in signaling mediated by Src kinases includes conformational activation and control of the equilibrium between active and down-regulated forms of Src. Tyrosine phosphorylation and intramolecular domain interactions are used in the cell to modulate this equilibrium, with maximum catalytic activity being achieved when the activation loop is phosphorylated and contacts between the catalytic domain (CD) and the regulatory SH2/SH3 domains are released (Sicheri and Kuriyan 1997; Boggon and Eck 2004). Nonetheless, some activity remains in the absence of loop phosphorylation (Porter et al. 2000; Adams 2003).

Normal cellular function requires tight control of Src kinase activity and the equilibrium between active and down-regulated conformations. Src kinases comprise SH3, SH2, and catalytic domains, flanked by N- and C-terminal tails. The end states of Src conformational activation are known from the considerable structural information accumulated for protein kinases and the Src family. The CD is highly conserved among all protein kinases, and the first view of this structure was reported for protein kinase A

Reprint requests to: Carol Beth Post, Medicinal Chemistry and Molecular Pharmacology Department, Markey Center for Structural Biology and Purdue Cancer Center, Purdue University, West Lafayette, IN 47907-2091, USA; e-mail: cbp@purdue.edu; fax: (765) 496-1189.

Abbreviations: CD, catalytic domain; SH2, Src homology domain 2; SH3, Src homology domain 3; CD_{act}, Lyn catalytic domain active conformation; CD_{down}, Lyn catalytic domain down-regulated conformation; N-lobe, N-terminal lobe; C-lobe, C-terminal lobe; MD, molecular dynamics; BMD, biased molecular dynamics; A-loop, activation loop; αC, α-helix C; RMSD, root mean squared deviation; α, pairwise force constant.

Article published online ahead of print. Article and publication date are at http://www.proteinscience.org/cgi/doi/10.1110/ps.051999206.

(Knighton et al. 1991). The structure of the activated form was determined for an isolated CD fragment from the Src family member Lck (Yamaguchi and Hendrickson 1996), and the down-regulated forms were first reported for constructs lacking only the N-terminal unique region of the two family members Hck (Sicheri et al. 1997) and Src (Williams et al. 1997; Xu et al. 1997). These studies not only revealed the key conformational differences between active and down-regulated forms of Src family CD but also defined for the first time how SH2 and SH3 contacts with CD influence activation.

The kinase catalytic domain has an N-terminal lobe (N-lobe) (Fig. 1, cyan and blue) and a C-terminal lobe (C-lobe) (Fig. 1, gold and red) separated by a deep cleft where ATP and substrate bind. The activation loop (A-loop) (Fig. 1, red) forms part of this cleft. Autophosphorylation of Tyr416 (chicken c-Src numbering is used throughout this report) on the A-loop activates Src in the cell (Barker et al. 1995). Several features distinguish this active CD conformation (CD_{act}) (Yamaguchi and Hendrickson 1996; Breitenlechner et al. 2005) from the down-regulated conformation (CD_{down}) (Sicheri et al. 1997; Williams et al. 1997; Xu et al. 1997, 1999; Schindler et al. 1999; Cowan-Jacob et al. 2005). The primary difference is the alternative conformations of the A-loop; in CD_{act} (Fig. 1A–C), the A-loop forms an extended structure that opens the cleft region to make the active site available for substrate binding. In contrast, the A-loop in CD_{down} (Fig. 1D–F) is more compact and forms two short α-helices that fill the cleft and thus occlude substrate. In addition, lobe–lobe orientation and the internal position of the α-helix (αC) differ. The orientation of the N- and C-lobes is more open in CD_{act} relative to that in CD_{down} so that the size of the cleft opening is increased. The internal variation in αC is the position of this helix within the N-lobe; αC in CD_{act} is displaced with respect to the β-sheet toward the interior of the protein.

Improper control of activation of different Src kinases has implicated members of the Src family in numerous disease states ranging from autoimmune diseases (Lowell et al. 1994; Lowell and Soriano 1996) to cancer (Verbeek et al. 1996; Lutz et al. 1998), with the result that Src kinases and other non–receptor protein tyrosine kinases are recognized to be key drug targets (Noble et al. 2004; Krause and Van Etten 2005). Inhibition by one effective treatment of chronic myelogenous leukemia, imatinib (Capdeville et al. 2002), is particularly noteworthy in that intermolecular recognition takes advantage of the structural

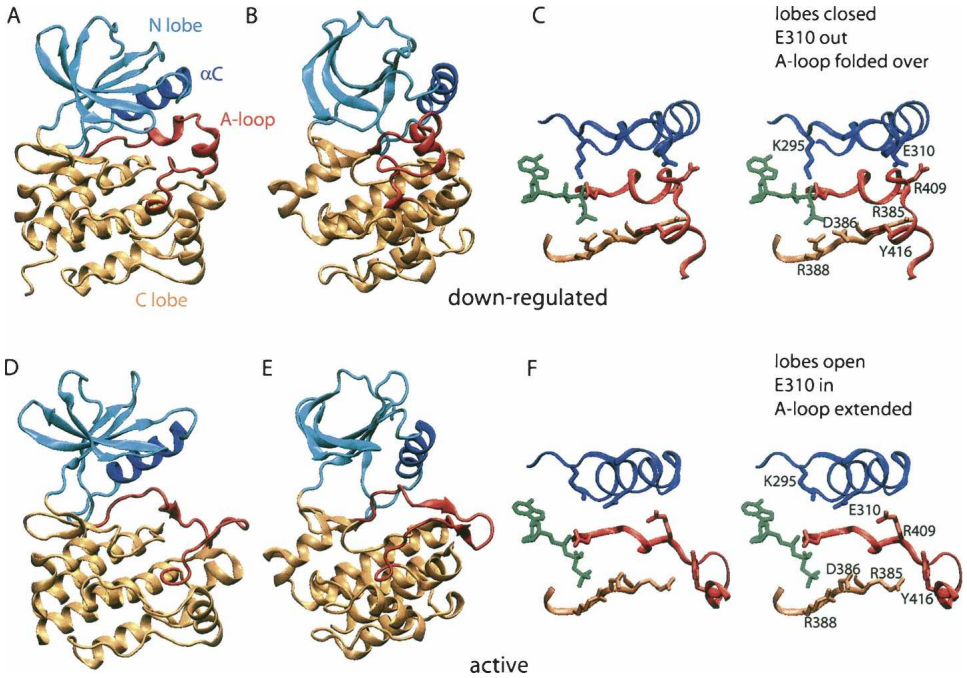

Figure 1. A comparison of the Lyn catalytic domain structures in the down-regulated (CD_{down}) (*A–C*) and active (CD_{act}) (*D–F*) conformations. The SH3 and SH2 domains are not shown. The structures are from equilibrium molecular dynamics simulations initiated with coordinates obtained by homology with Lck (Yamaguchi and Hendrickson 1996) and Hck (Schindler et al. 1999) crystal structures. *B* and *E* are rotated 90° with respect to *A* and *D*. The N-lobe is shown in cyan, the C-lobe in gold, and αC in blue. The A-loop (red) extends away from the catalytic site in CD_{act} and folds over in CD_{down}, occluding the substrate-binding site. Stereoview of the cleft region illustrates the important interactions, listed in Table 1, for CD_{down} (*C*) and CD_{act} (*F*) conformations. ATP is shown in green; the C-lobe residues in gold; the A-loop in red; and N-lobe residues, including the helix αC, in blue. The structure figures were generated using VMD (Humphrey et al. 1996).

differences associated with conformational activation (Schindler et al. 2000).

One approach to overcome problems with specificity, and to find more effective inhibitors, is to gain a better understanding of the physical behavior of kinases including the process of kinase conformational activation. To this end, computational studies of a Src-family member, Lyn kinase, were conducted and reported here. The sequence and structural similarities among Src kinases and protein kinases in general imply that deciphering the activation mechanism of one Src kinase will afford clues about the activation mechanism of the Src-family and other kinases. Lyn initiates (Burkhardt et al. 1991; Yamanashi et al. 1991) and down-regulates (Chan et al. 1997, 1998; Nishizumi et al. 1998; Smith et al. 1998; Hong et al. 2002) B-cell signaling. NMR studies to examine substrate recognition of Lyn for ITAM have been reported (Gaul et al. 2000).

The structures of CD_{down} (Sicheri et al. 1997; Xu et al. 1997) and CD_{act} (Yamaguchi and Hendrickson 1996) provide the starting point for understanding the mechanism of kinase activation, although the static crystal structures give information on neither the order nor the interdependence of conformational changes that must occur for activation. Certain features of conformational activation have been inferred from these two end states. It has been suggested that intramolecular domain–domain contacts stabilize CD_{down} by either hindering αC motion, thus preventing the A-loop displacement required for activation (Schindler et al. 1999), or by stabilizing the closed conformation of the catalytic domain lobes and keeping the A-loop tyrosine inaccessible (Xu et al. 1999). The computational study reported here aims to begin to elucidate the conformational transition between CD_{down} and CD_{act} and to define the interdependence between displacements in αC, the A-loop, and lobe–lobe orientation.

Biased molecular dynamics (BMD) was used to study the conformational transition between CD_{act} and CD_{down}. The time scale for this transition has been measured for protein kinase A to be in the 5–6-msec range (Shaffer and Adams 1999). With BMD, a biasing potential is added to the molecular mechanics force field in order to study this transition within a computationally feasible time scale. The biasing potential moves the protein toward a target structure, and is added as a global sum over the system so that departures in local structure away from the target are allowed as long as the cumulative motion is in the desired direction. The consistent characteristics of the pathways from several trajectories can give information about possible energy barriers (Neria et al. 1996). Similar methods to study activated processes are targeted molecular dynamics (TMD) and steered molecular dynamics (SMD). For BMD, the potential is like a ratchet in that it is added only when the system moves away from the target, whereas in TMD and SMD the potential is present at all times. This feature of BMD is expected to be advantageous by allowing the system to follow the energy surface more closely. BMD has been previously used to study unfolding (Marchi and Ballone 1999; Paci and Karplus 1999; Morra et al. 2003) and dissociation (Paci et al. 2001; Li et al. 2005). TMD and SMD have been used to study the conformational changes of GroEL (Ma et al. 2000) and Ras (Diaz et al. 1997; Ma and Karplus 1997) and unbinding of avidin-biotin (Israelewitz et al. 2001a). TMD has also been used to examine certain features of the Src kinase conformational transition. These studies primarily focus on the role of the SH3–SH2 linker in coupling domains (Young et al. 2001) and the structural effects of the N-terminal residues of CD in interdomain communication (Banavali and Roux 2005).

We examined the unphosphorylated, isolated catalytic domain of Lyn for this initial computational analysis of activation. The Src-family catalytic domain is constitutively active (Yamaguchi and Hendrickson 1996) and inhibited by small molecules to a similar extent as the full-length form (Zhu et al. 1999). In addition, Src kinase activity is observed in the absence of Tyr416 phosphorylation (Porter et al. 2000; Adams 2003). Therefore, the catalytic domain captures significant features of conformational activation, and a description of the transition behavior in the absence of phosphorylation on Tyr416 provides information on the underlying physical processes involving the overall structure. Computational investigations should also give insight into the structural basis for conformationally selective ligand binding (Schindler et al. 2000; Kwak et al. 2005), and thus assist in the development of new kinase inhibitors. The key result from the analysis of the BMD simulations is that the network of electrostatic interactions in CD_{down} switches to an alternative network in CD_{act} so that the transition may be described as a switched electrostatic network. A set of six polar or charged residues consistently switch in a temporally short fashion between binding partners over the course of the transition. These residues are highly conserved, and some are already assigned important roles in catalysis or binding. We propose that these residues also serve central roles in the transition process by functioning as a switched electrostatic network to guide the transition as anchor points along the pathway.

Results and Discussion

Equilibrium simulations

Equilibrium MD simulations in explicit solvent were calculated as described in Materials and Methods for Lyn catalytic domain conformations CD_{act} and CD_{down} in the presence or absence of ATP. The calculations were first performed with an implicit representation of water (effective energy function) (Lazaridis and Karplus 1999); however, the structures deviated by >3 Å from the crystal

Table 1. *Important residue interactions that define the active and the down-regulated conformations of the kinase domain*

Residue	Location	Active[a]	Inactive[b]
K295	N lobe	E310	D404, ATP
E310	Helix αC	K295	R409, Y382
D386	Catalytic loop	R388, N391	R388, N391, Y416
D404	Metal-binding loop	Mg^{2+}	Mg^{2+}, K295
R409	A-loop	Y416	E310
Y416	A-loop	R409, R385	D386
ATP	Within catalytic cleft	R388	R388, K295

[a] Interacting partner in the active state.
[b] Interacting partner in the inactive state.

structure at the end of 1 nsec (data not shown). In addition to establishing the stability of the simulation systems, the equilibrium simulations served to generate target structures equilibrated to the CHARMM22 force field for each conformational end state. The equilibrium simulations were stable over time with respect to temperature, energy, and structure. The RMS difference of the simulation structures against the initial structure reaches a plateau after 0.2 nsec and remains constant throughout the 0.3- to 0.4-nsec trajectories. After superposition of the whole catalytic domain, the RMS deviations in the backbone atoms N, C_α, and C at the end of the equilibrium simulations were ~1.5 Å relative to the initial structure for both active and down-regulated catalytic domains.

The key interactions that distinguish CD_{act} and CD_{down} (Yamaguchi and Hendrickson 1996; Schindler et al. 1999; Xu et al. 1999) are summarized in Table 1 and illustrated in Figure 1, C and F. These interactions were stable throughout the equilibrium simulations. In CD_{act}, the A-loop is extended away from the active site, in a conformation that allows substrate access to the active site. In this extended conformation, the phosphoryl group of pTyr416 on the A-loop interacts with Arg385 and Arg409. In CD_{down}, the A-loop is folded over the active site, and Tyr416 then forms a hydrogen bond with Asp386 in the catalytic site. Glu310 was recognized to be a key residue associated with the alternative orientations of αC (Schindler et al. 1999; Xu et al. 1999). In CD_{act}, where αC is turned in toward the ATP binding site, Glu310 interacts with the catalytically critical residue Lys295 (Snyder et al. 1985; Kamps and Sefton 1986). Alternatively, the outward rotation of αC in CD_{down} places Glu310 in close contact with Arg409 and Tyr382. The A-loop and αC are located at the interface of the N- and C-lobes of the catalytic domain so that their alternative structures would influence the conformation of the third distinguishing feature, the disparate lobe orientations.

The pathway calculations described in this study were performed on the Lyn catalytic domain without phosphorylation of Tyr416 in order to retain the same chemical structure for the two end states, CD_{act} and CD_{down}. The stability of the A-loop structure with unphosphorylated Tyr416 in the context of the active conformation of the catalytic domain was therefore assessed by comparing equilibrium simulations of CD_{act} with Tyr416 either phosphorylated or unphosphorylated. The set of electrostatic interactions around phosphotyrosine includes two arginines, Arg409 and Arg385. These interactions are stable in the equilibrium simulation with phosphorylated Tyr416. For simulations in which Tyr416 is not phosphorylated, Arg409 and Arg385 side chains are in van der Waals contact with Tyr416, and the electrostatic interactions are maintained. Thus, unphosphorylated Tyr416 in CD_{act} does not result in a large perturbation of the A-loop conformation in the time period of the simulations. In a recent structure of unphosphorylated Src kinase in the active conformation, the contacts between Tyr416 and the two arginines are also maintained (Cowan-Jacob et al. 2005).

Biased molecular dynamics

Forward and reverse transitions between CD_{act} and CD_{down} were calculated with values of the pairwise force constant, α, equal to 0.0004, 0.0009, 0.0013, and 0.0022 kcal/(mol $Å^4$) with and without ATP (Table 2). At the largest α-value, the force on a single atom of the biased set ranged from 0 to ~150 pN. This value is at the lower end of the previously reported range of 100–500 pN (Paci and Karplus 1999). The initial and target structures used for the biased MD simulations of the catalytic domain were those obtained following 0.3–0.4 nsec of equilibrium

Table 2. *Summary of BMD simulations*

Transition	α[a]	Duration (nsec)	RMSD (Å)[b]	*R* (Å)[c]
No ATP				
$CD_{down} \rightarrow CD_{act}$	4	1.9	2.06	1.95
$CD_{down} \rightarrow CD_{act}$	9	1.9	2.26	2.28
$CD_{down} \rightarrow CD_{act}$	13	1.7	1.78	1.43
$CD_{down} \rightarrow CD_{act}$	22	1.5	1.68	1.29
$CD_{act} \rightarrow CD_{down}$	4	1.9	2.24	2.5
$CD_{act} \rightarrow CD_{down}$	9	1.8	1.94	1.94
$CD_{act} \rightarrow CD_{down}$	13	1.5	1.89	1.91
$CD_{act} \rightarrow CD_{down}$	22	1.3	1.65	1.52
With ATP				
$CD_{down} \rightarrow CD_{act}$	4	1.9	2.56	2.82
$CD_{down} \rightarrow CD_{act}$	9	1.4	2.13	2.07
$CD_{down} \rightarrow CD_{act}$	13	1.6	1.84	1.51
$CD_{down} \rightarrow CD_{act}$	22	1.4	1.85	1.47
$CD_{act} \rightarrow CD_{down}$	4	1.4	2.46	3.00
$CD_{act} \rightarrow CD_{down}$	9	1.7	2.03	2.15
$CD_{act} \rightarrow CD_{down}$	13	1.5	1.69	1.6
$CD_{act} \rightarrow CD_{down}$	22	1.5	1.79	1.74

[a] Pairwise force constant value in 10^4 kcal/(mol $Å^4$).
[b] RMSD of CD heavy atoms between the target and the average structure from the last 10 psec of simulation.
[c] Reaction coordinate value (Equation 1).

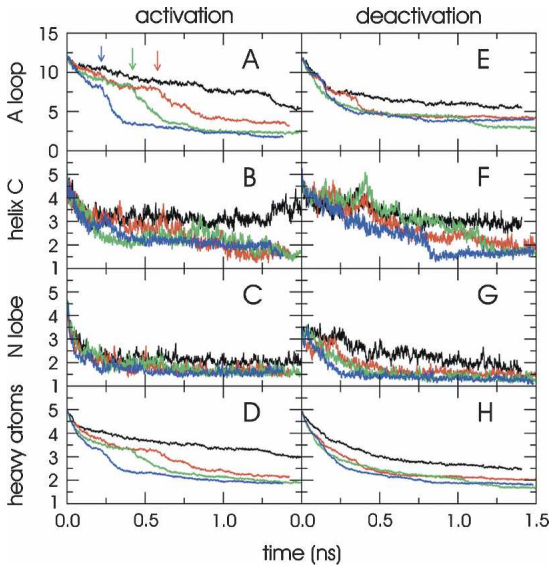

Figure 2. Progress curves for activation (*A–D*) and deactivation (*E–H*) in the presence of ATP with the pairwise force constant $\alpha = 0.0004$ (black), 0.0009 (red), 0.0013 (green), and 0.0022 (blue). From the *bottom*, the time profiles of the RMSD of the simulation structures to target structure for all (*D,H*), for the N-lobe (*C,G*), for helix αC (*B,F*), and for A-loop (*A,E*) heavy atoms are shown. The heavy atom RMSD is calculated after superpositioning all CD heavy atoms, and the structural element RMSD values are calculated after superpositioning based on the C-lobe α-helices. The arrows in *A* indicate the point of change in slope for the A-loop RMSD.

MD. No significant effect of ATP on the conformational transition was found.

The progress of the biased simulations for Lyn calculated using different α-values is shown in Figure 2 with the transitions for activation ($CD_{down} \rightarrow CD_{act}$) on the left-hand side, and those for deactivation ($CD_{act} \rightarrow CD_{down}$) on the right-hand side. The RMSD to the target structure is plotted as a function of time for all heavy atoms (Fig. 2, bottom panel), and for a subset of residues to indicate the individual progress of the three structural features of the conformational transition (Fig. 2, top three panels). The RMSD for the three structural elements are calculated after superposition of the structures with respect to the α-helices in the C-lobe. The RMSD is averaged over heavy atoms of the element: residues 403–429 for the A-loop, 304–314 for αC, and 261–341 excluding αC residues for the N-lobe.

The RMSD to target structure for all heavy atoms decreases from starting values of ~5 Å to limiting values of ~2 Å within 1.5 nsec for most simulations. The largest conformational difference occurs for the A-loop, which has a 12 Å initial RMSD that levels off at 2.5–5 Å. Small increases in RMSD values are observed along the pathway for certain elements, particularly for αC. The biased MD method therefore can tolerate increases in the RMSD value for a subset of atoms even though the global target RMSD value [R(t)] is restrained to decreasing values. As such, transient moves away from the target are possible for local regions if dictated by the potential surface.

Conformational transition is nonuniform

Decay profiles of the RMSD progress curves calculated for a subset of residues show that the conformational transition does not occur uniformly throughout the catalytic domain. The decay profiles vary for the A-loop, αC, and the lobe orientation (Fig. 2, top three panels), as well as for the activation transition and the reverse deactivation transition (left vs. right column). The opening of the two lobes (Fig. 2C) in the activation transition occurs early, within an ~50-psec time period. Closing down of the lobes in the transition to CD_{down} (Fig. 2G) is considerably slower, requiring as long as 250 psec, and shows a dependence on the value of the pairwise force constant, α. The activation and deactivation transitions for αC differ in a similar fashion. The αC activation curves (Fig. 2B) decay relatively smoothly and early in the transition, whereas the progress toward CD_{down} (Fig. 2F), with Glu310 rotated out, is slower and shows a stronger dependence on α. The largest conformational change occurs in the A-loop. The A-loop activation transition (Fig. 2A) is interestingly more complex than the N-lobe and αC transitions are and consistently shows biphasic behavior that depends on the magnitude of α.

Differences in the N-lobe and αC decay profiles shown in Figure 2 can be rationalized from a simple mechanical view of the structural changes. Comparison of the structures for CD_{act} and CD_{down} finds that the N-lobe is reoriented relative to the C-lobe by a simple rigid-body motion except for the position of αC (Fig. 3). The change in αC, observed after superpositioning the C-lobes, is rotation about the helix axis and translation of the N-terminal end of αC relative to the β-sheet of the N-lobe. The lobe opening during activation occurs relatively fast, and the RMSD decays monotonically, characteristic of an unhindered hinge opening. This opening is accompanied by unimpeded inward rotation and translation of αC toward the ATP-binding site (Fig. 3, gold). This internal displacement of αC explains the slower progress for lobe closure relative to opening (Fig. 2, cf. F,G and B,C); lobe closure, to generate CD_{down}, depends on rotation of αC to the "out" position to allow room for the lobes to close, while lobe opening can proceed independent of the position of αC. Further, the αC-in conformation is not compatible with the A-loop conformation folded over the active site in CD_{down} as shown by the steric clash in Figure 3 between the gold αC and the blue A-loop. Correspondingly, folding the A-loop over the active site to reach the CD_{down} conformation must cooperate with rotation of αC to the out position. Thus, the kinase

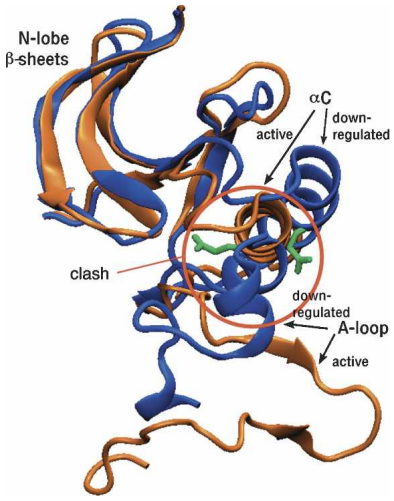

Figure 3. Ribbon drawing of the N-lobe (β-sheet and αC) and the A-loop to illustrate the interdependent motion of the A-loop and αC. CD_{down} conformation of the A-loop (blue) clashes with the CD_{act} conformation of helix αC (gold). The N-lobe, including αC and the A-loop, is shown for CD_{act} (gold) and CD_{down} (blue). The Glu310 side chain is shown in green. The clash site is indicated by a circle. The superposition of CD_{act} and CD_{down} is based on the N-lobe β-sheets.

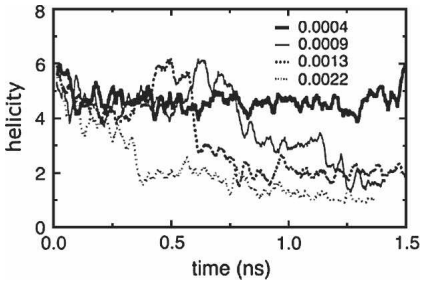

Figure 4. The A-loop helix unwinding during activation appears to be a barrier. The helicity measures the number of residues in the helical region of conformational space for residues 413–422 of the A-loop. A running average with a 25-psec window is shown for the trajectories. The drop in helicity corresponds to the drops in the RMSD to target plots for the A-loop in Figure 2.

deactivation/activation mechanism involves interdependent displacements of αC, the N-lobe, and the A-loop (Schindler et al. 1999; Xu et al. 1999).

A-loop transition

The transition to open the A-loop and expose the active site has multiple components (Fig. 2A). An initial decay in RMSD against the target structure is followed by a more rapid decrease that occurs at times depending on the value of the pairwise force constant α. The strong dependence on α is consistent with an energy barrier to the conformational change that underlies the drop in RMSD value. Analysis of the trajectories finds the α-dependent decrease to be a helix–coil transition in the short 1.5-turn α-helix in the C-terminal end of the A-loop, residues 413–422. The time dependence of the helicity, monitored from the number of residues with main-chain dihedral angles in the helical region, is shown in Figure 4. Unwinding of the short helix corresponds in time with the drop in RMSD of the A-loop. By visualization of the trajectories, the A-loop is observed to open out from the two ends, and the helix then unwinds concertedly. Further, immediately prior to helix unwinding (Fig. 2A, arrows), similar Lyn CD structures are observed independent of α, so that a consistent intermediate (Fig. 5) exists in the transition. Preceding helix unwinding, the catalytic domain main chain overlays well in all parts of the catalytic domain including the A-loop. The similarity in these intermediate structures suggests that a bottleneck in a common activation pathway involves helix unwinding of the A-loop of Lyn CD. Tyr416 is on this helix of the A-loop, and the side chain faces into the active site in the down-regulated state. Interestingly, when the A-loop opens out in the activation simulations, the Tyr416 side chain is transiently exposed to solvent. The helix–coil transition may facilitate exposure of Tyr416 to make it available for phosphorylation.

In the case of deactivation, the progress curves for the A-loop folding over the active site (Fig. 2E) show an initial decrease in RMSD with a small-amplitude second decay in some, but not all, trajectories. Beginning with the A-loop extended on the C-lobe surface, two β-sheet interactions with the C-lobe are broken rapidly, with subsequent reorientation of the loop between them. Although there is a rapid drop in RMSD from 12 Å to 4–5 Å, the transition to the active state of the A-loop is not complete

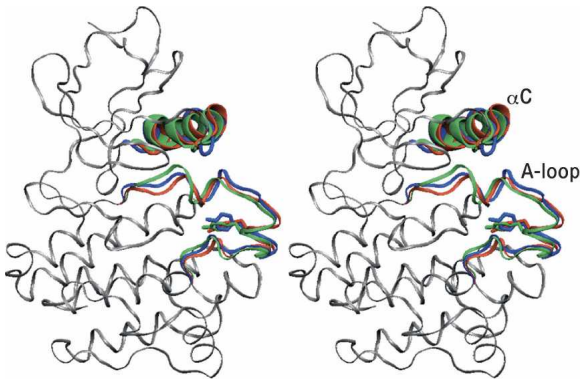

Figure 5. Intermediate conformations from BMD are similar as shown by the stereo view of the structures from multiple trajectories at the time points corresponding to the arrows in Figure 2A. The ribbon representation of the main chain is in gray for the trajectory calculated with $\alpha = 0.0009$. The A-loop and αC are shown for structures that were calculated with $\alpha = 0.0009$ (green), $\alpha = 0.0013$ (red), and $\alpha = 0.0022$ (blue).

within the simulation time; the RMSD value plateaus at ~4 Å and the short helix is not formed. The incomplete folding of the A-loop over the active site may be the result of a significant energy barrier to helix formation, or may be a limitation of the methodology in view of the steric conflict with αC described above.

A switched electrostatic network links the A-loop with αC and active-site residues

Trajectories were analyzed to identify interresidue interactions that were consistently formed/broken over the course of the transitions and thus likely to serve a functional role in kinase conformational activation. Rather than independent pairwise interactions, this analysis identified a group of polar residues that form alternative networks of interaction in CD_{down} and CD_{act}. One set of interactions was observed to exchange with the alternative set for these polar residues, suggesting that these residues function like an electrostatic switch to guide the activation/deactivation transition. The switch, shown schematically in Figure 6, comprises a group of six residues: the catalytic Asp386, the regulatory Tyr416 on the A-loop, Arg409 on the A-loop, Glu310 on αC, the functionally critical Lys295, and Asp404 of the metal-binding DFG sequence. The four central residues—Tyr416, Arg409, Glu310, and Lys295—exchange binding partners to switch between a three-way and a two-way network. These six residues are highly conserved among kinases, and some have been

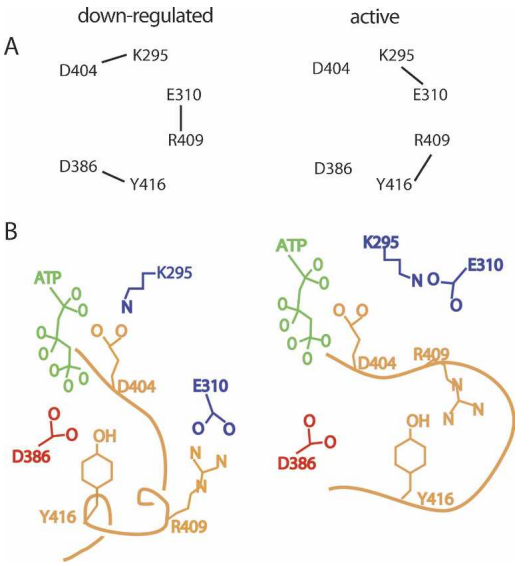

Figure 6. A network of residues links the A-loop, αC, and the active site. The residues switch during activation between a three-way network of interactions in CD_{down} (*left*) and a two-way network in CD_{act} (*right*). The network is shown in *A* and a schematic diagram is shown in *B*. N-lobe residues are in blue, the A-loop is in gold, and C-lobe residues are in red.

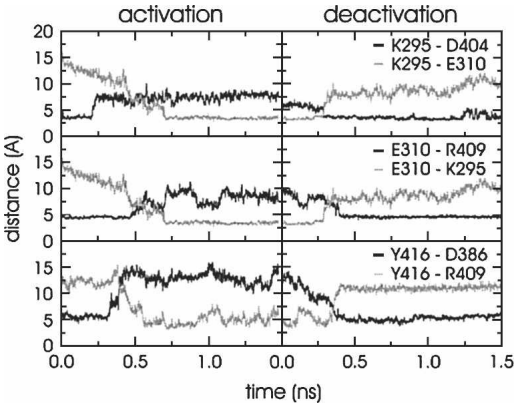

Figure 7. Distances between the residues involved in the switch mechanism. Distances (Å) between Tyr416–Arg409 (black) and Tyr416–Asp386 (gray) are given in the *bottom* panel. The *middle* panel depicts the distances between Glu310–Arg409 (black) and Glu310–Lys295 (gray). The *top* panel shows the distances between Lys295–Asp404 (black) and Lys295–Glu310 (gray). The interresidue distances are between the polar atoms of least separation. The activation calculation with $\alpha = 0.0022$ and the deactivation calculation with $\alpha = 0.0013$ are shown.

recognized for distinguishing the active and the down-regulated states (Yamaguchi and Hendrickson 1996; Schindler et al. 1999; Xu et al. 1999). The down-regulated state is the three-way network (Asp386–Tyr416, Arg409–Glu310, Lys295–Asp404) (see Fig. 6B), which links the A-loop to either the N- or the C-lobe (Fig. 6A). When the A-loop opens toward the active form, these interactions switch to two alternative ones within the A-loop (Tyr416–Arg409) and within the N-lobe (Glu310–Lys295).

This group of residues was identified from the switch-like nature of interactions apparent in the time profiles of interaction distances or energy. There is an exchange of the alternative CD_{act} and CD_{down} interactions whereby the formation of one follows closely in time with the loss of the other. The behavior is illustrated in Figure 7 with the switch of Tyr416 between Asp386 and Arg409, of Glu310 between Arg409 and Lys295, and of Lys295 between Asp386 and Glu310. In the case of the transition from CD_{down} to CD_{act} and Tyr416 (Fig. 7, bottom left panel), the initial interaction with Asp386 is retained for ~0.3 nsec, when the alternative interaction with Arg409 is formed. For simulations initiated from CD_{act} and biased toward CD_{down} (Fig. 7, bottom right panel), the reverse exchange of interactions takes place. The same type of switching behavior is shown for Glu310 and Lys295 as the central switching residues (Fig. 7, top panels).

Similar patterns in the exchange of interactions for the central residues occurred for the majority, but not all, of the time profiles from the biased trajectories. In a small number of biased simulations, some exchanges did not occur, and the original interactions were retained throughout the biased trajectory. The Glu310–Arg409 to Glu310–Lys295

switch showed the greatest variation, shown by the time profiles from several trajectories in Figure 8. In two out of eight trajectories the exchange did not occur.

The interactions of the electrostatic switch appear to function as anchor points that guide the conformational change over the course of the transition. The conformational changes of the A-loop and αC are large internal motions, yet the interresidue distances between the switch residues remain comparatively short and constant until the point of the exchange. The distance Glu310 to Arg409 remains short even when the A-loop opens out (Fig. 9, middle panels), then Glu310 switches to interact with Lys295 (Fig. 9, bottom panel). Thus, the side-chain interactions serve as anchor points in the transition. The short-range interactions "float" with the main-chain displacement until the exchange with the alternative partner.

In addition to those proposed for the electrostatic switch, there are, of course, several other electrostatic interactions that differ between the active and the down-regulated forms of Src kinase. Indeed, the six switch residues interact with other residues not included in Figure 6. The specific interactions proposed here for the electrostatic switch are suggested to be the critical ones for guiding the conformational transition based on a temporally close exchange of the central residue interacting with one partner to the second. In other cases of different binding partners in CD_{act} and CD_{down}, the two interactions were either both broken or formed simultaneously over the course of most transition trajectories.

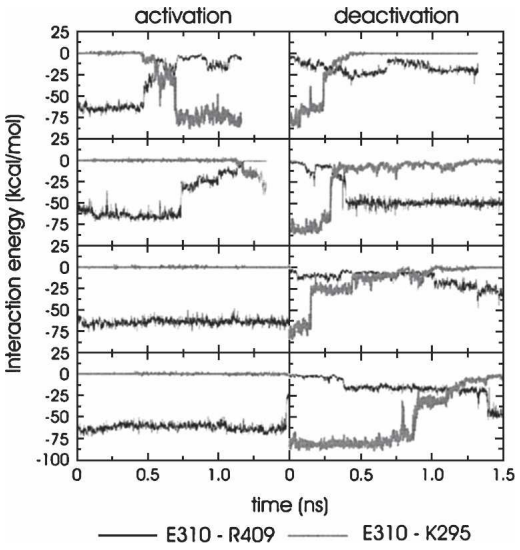

Figure 8. Glu310–Arg409 (black) and Glu310–Lys295 (gray) interaction energies (electrostatic + vdW) for the activation and the deactivation calculations. Only in those activation simulations where Glu310–Arg409 breaks does the helix rotate and Glu310–Lys295 form. The Glu310–Arg409 interaction is hard to break in activation; on the other hand, it forms rapidly in the deactivation calculations.

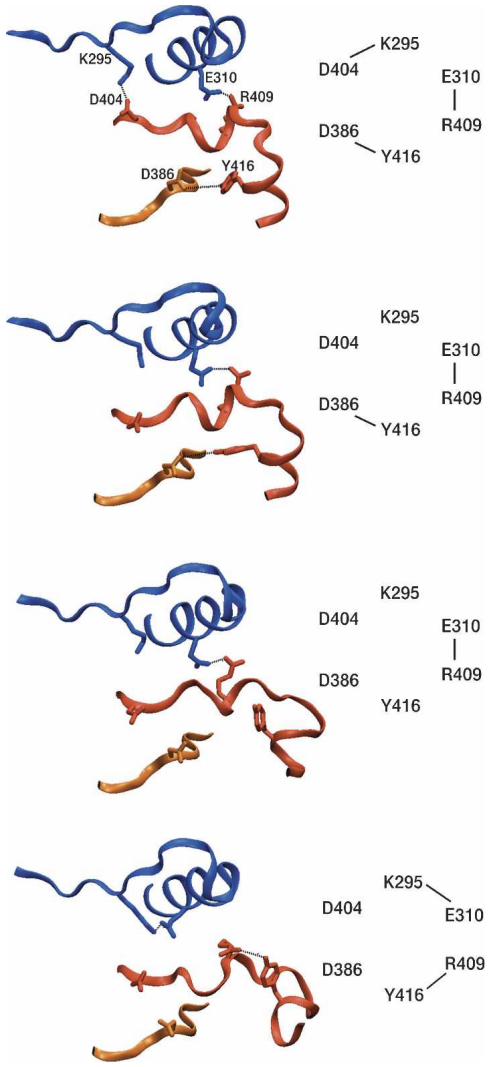

Figure 9. The switched electrostatic network in activation. From the *top*, snapshots at 100 psec, 250 psec, 400 psec, and 750 psec from the activation calculation with $\alpha = 0.0022$ are shown. αC that has the Glu310 and β5 that has the Lys295 are in blue, the A-loop with Arg409 and Tyr416 is in red, and the catalytic loop with Asp386 is in gold. Tyr416 switches from Asp386 to Arg409 as Glu310 switches from Arg409 to Lys295 during the simulation. Distances <5 Å are shown with dotted lines for the network residues.

Conclusions

Biased molecular dynamics simulations were used to obtain an initial description of the conformational transition between the active and the down-regulated states of unphosphorylated Src kinase catalytic domain, and thus provide the groundwork for more detailed study of the energetics of the activation pathway.

BMD and other similar methods (TMD [Schlitter et al. 1993] and SMD [Isralewitz et al. 2001b]) that use an additional potential to overcome energy barriers and move from one state to the other in nanoseconds are useful in

studying conformational transitions that may take place in microseconds to seconds in the cell. Such nonequilibrium methods make it possible to determine pathways and energy barriers for these conformational transitions. The underlying energy landscape guides the transition; however, the sequence or relative timescales of events in the pathway is dependent on the magnitude of the potential as applied to a selection of atoms, with higher forces resulting in greater loss of temporal detail (Bryant et al. 2000). We used different force constants to study the forward and the reverse transition for activation in order to obtain the consistent characteristics. Our results describe conformational features for CD activation and certain aspects of interdependence among them, rather than the specific sequence with which they take place.

We find that the activation and deactivation transition of CD progresses nonuniformly. The opening of the two lobes occurs early in the activation transition and is unimpeded. An intrinsic flexibility in the lobe–lobe orientation has also been deduced from crystallographic analyses of Src kinase structures whereby the *B*-factors associated with the N-lobe were twice as high as those of the C-lobe (Breitenlechner et al. 2005). On the other hand, a helix–coil transition in the A-loop is slower and appears to be hindered by an energy barrier. The reverse deactivation transition is complicated by the interdependence of the outward rotation of αC and the folding of the A-loop over the active site.

Elucidation of the pathway at the detailed atomic level allowed only by computation is valuable for understanding the enzymatic activity of protein kinases without A-loop phosphorylation (Porter et al. 2000; Adams 2003) and inhibition by conformationally selective compounds such as imatinib (Capdeville et al. 2002) and gefitinib (Kwak et al. 2005). Intramolecular domain–domain interactions are thought to deactivate Src kinase by locking the lobe orientation or by stabilizing the inactive conformation of αC. It has been suggested that when the lobes open, Tyr416 becomes accessible for phosphorylation (Xu et al. 1999). The fast and facile opening of the lobes observed in this study of CD without the SH2/SH3 regulatory domains indicates that this suggestion is indeed reasonable. The ease of lobe reorientation and the electrostatic switch mechanism that functions in the transition in the absence of phosphorylation suggest that the active conformation is transiently populated by kinase absent of A-loop phosphorylation and bound inhibitor. Thus, we propose that the activity of Src unphosphorylated on the A-loop (Porter et al. 2000; Adams 2003) arises from the transient formation of CD_{act} rather than another conformation of the kinase of lower catalytic power. Stabilization of CD_{act} relative to CD_{down} likely requires phosphorylation of the A-loop tyrosine. A similar behavior was observed for NtrC in which phosphorylation shifts the equilibrium rather than inducing a new structure (Volkman et al. 2001). From the interdependence of the displacements in the A-loop and αC and the time dependence of the Glu310 exchange between Arg409 and Lys295 in BMD, we conclude that phosphorylation of Tyr416 would stabilize not only the A-loop but also αC conformations in CD_{act}.

A major outcome of this investigation is the proposal that the transition is conformationally controlled by a switched electrostatic network involving the exchange between a three-way and a two-way network of interactions among Asp386, Tyr416, Arg409, Glu310, Lys295, and Asp404. The switch residues are highly conserved in tyrosine kinases, suggesting that this switched network may play an important role in other kinases as well. The ATP-binding Lys295, metal-binding Asp404, and catalytic Asp386 are absolutely conserved. Arg409 is absolutely conserved across the Src kinase family and functionally conserved across the kinase family. Helix αC Glu310 is highly conserved if not strictly conserved across all kinases. Our analysis suggests that the same residues essential for either structural stabilization (Yamaguchi and Hendrickson 1996; Schindler et al. 1999; Xu et al. 1999) or for catalysis (Kamps and Sefton 1986; Gibbs and Zoller 1991; Porter et al. 2000) also play important roles in the transition between the two end states.

The six residues of the network exchange from one group to another when the A-loop main chain extends out and refolds, and thus serve as anchor points to guide the conformational transition. Interactions in CD_{down} of Tyr416 and Arg409 on the A-loop connect to active-site residues and to αC, and link the A-loop conformational change to the reorientation of the N- and C-lobes and to the displacement of αC (Fig. 9). Further, the switch centered on Glu310 is likely to be energetically significant to the conformational change of the A-loop and αC. The Glu310–Arg409 interaction impedes rotation of αC and the inward positioning of Glu310 for activation. This interaction seems particularly stable since it breaks late in the activation process where αC rotates in, and forms early in the reverse deactivation process (Fig. 8). Phosphorylation of Tyr416 would likely shift the equilibrium in favor of the Glu310–Lys295 position of the switch in CD_{act} by competing to form the Try416–Arg409 interaction and thus release Glu310 to interact with Lys295. The electrostatic network, therefore, offers a mechanism for conformational activation, whereby phosphorylated Tyr416 on the A-loop could influence not only the change in the A-loop conformation but also the conformational transition throughout the catalytic domain. It is of interest to know how concerted the exchanges are for the four central residues, but the concertedness could not be determined from the current sampling in the biased simulations.

The switched electrostatic network mechanism proposed here concerns the conformational activation of protein kinases in contrast to earlier discussions of electrostatic

switches for equilibrium states. Previous studies on Src kinases (Xu et al. 1999) recognized the switch in interactions between the two crystallographic structures of active and down-regulated kinases and their role in stabilization of two conformational states. The current study expands the roles proposed for these critical residues to include stabilization of the conformational transition. The term ''electrostatic switch'' has also been used to describe a change in the binding equilibrium of Src kinases (McLaughlin and Aderem 1995), whereby phosphorylation of the N terminus was shown to enhance membrane-binding affinity and reverse the relative binding affinity between membrane-bound or cytoplasmic states of Src kinase.

Given the high conservation in the switch residues in the kinase family, the exchange pathway between active and down-regulated forms could be generally conserved in kinases. Conservation of conformational transition pathways has been suggested from evolutionary relationships for other proteins (Süel et al. 2003; Zheng et al. 2005). Slight variations in kinase catalytic domain structure, such as the A-loop conformation or relative lobe–lobe orientations, may result in differences in the order of events.

The presence of a switched electrostatic network in conformational activation can be tested experimentally providing conditions are established where conformational activation is a component of the rate-limiting step (Adams 2003). Kinetic assays on Src (Barker et al. 1995) and the Src-family kinase Hck (Moarefi et al. 1997) show that enzymatic activity exhibits an enzyme concentration-dependent lag phase, which can be eliminated by pre-incubation with MgATP. As the lag phase is likely dependent on conformational activation, dependence of the lag phase on salt concentration can provide information about the effect of the electrostatic switch on the enzyme mechanism. Similar kinetic studies to those reported are currently under way in the laboratory of our collaborator.

Materials and methods

Simulation systems

Initial coordinates of the active and the down-regulated conformations of the Lyn catalytic domain, residues 252–523, were obtained using the homology modeling program MODELLER 4.0 (Sali and Blundell 1993) based on the active Lck catalytic domain structure (3LCK.pdb; Yamaguchi and Hendrickson 1996) and the down-regulated Hck kinase structure (1QCF.pdb; Schindler et al. 1999), respectively. The sequence identity of Lyn with Lck is 73%, and the sequence identity with Hck is 82%. For proteins with sequence identities >40%, homology modeling can be used to predict the atomic structure with high accuracy (Rost 1999). For simulations with ATP and Mg^{2+}, the AMPPNP conformations in the down-regulated Src kinase structure (2SRC.pdb; Xu et al. 1999) and in the active Lck kinase structure (1QPC.pdb; Zhu et al. 1999) were used to place the ATP. The protein, with or without the ATP and Mg^{2+} bound, was then solvated in an equilibrated rhombic dodecahedron water box carved from a cubic box of 116 Å on one side with at least 14 Å of water between the protein coordinates and the edge of the box resulting in ~42,000 atoms.

Equilibrium simulations were calculated over 0.3–0.4 nsec with starting structures for unphosphorylated Lyn CD_{act} and CD_{down} with or without ATP and Mg. Simulations were also calculated for CD_{act} with the A-loop Tyr416 phosphorylated. To eliminate effects that could result from the force field, the unphosphorylated equilibrated structures were the initial and the target conformations used in biased molecular dynamics. The structures used were without A-loop tyrosine phosphorylation in order to have the same chemical structure for both starting and target conformations. The use of unphosphorylated end states provides the basis for deciphering the molecular details of the activation pathway without the chemistry step.

Molecular dynamics simulations were calculated with the CHARMM program (Brooks et al. 1983) using the CHARMM22 potential energy function (MacKerell et al. 1998) for the all atom model and TIP3P water parameters (Jorgensen 1981). Phosphotyrosine parameters were those of Feng et al. (1996). Periodic boundary conditions with the particle mesh Ewald method (Darden et al. 1993) were imposed on the system, and the nonbonded van der Waals interactions were truncated at 14 Å. A time step of 1 fsec was used with the leap-frog algorithm. SHAKE was used to constrain bonds to hydrogen atoms. A uniform dielectric constant of 1 was used throughout the study. The system was energy-minimized and subsequently equilibrated with the protein atoms constrained for the first 100 psec. All calculations were performed in the NPT ensemble at a constant pressure of 1 atm and constant temperature of 300 K with the Hoover method (Hoover 1985). Coordinate sets were saved every picosecond for analysis. Twenty picoseconds of BMD calculations required ~1 d of CPU time on two IBMSP processors (RS6000 375 MHz).

Biased molecular dynamics

The conformational transition pathway was studied by biased molecular dynamics (BMD) (Marchi and Ballone 1999; Paci and Karplus 1999). Application of a biasing potential promoted a conformational transition between the given starting structure and the target structure, and the crossing of the conformational space separated by energy barriers that cannot be overcome in regular MD. The external potential depends on the difference in the internal distances in the simulation and target structures and favors the decrease in its value. The reaction coordinate, R(t), is defined as

$$R(t) = \frac{\sum_{i=1}^{n} \sum_{j=i+1}^{n} [r_{ij}(t) - r_{ij}^{T}]^2}{N} \quad (1)$$

where $r_{ij}(t)$ is the pairwise distance between atom i and j coordinates at time step t, and r_{ij}^{T} is the pairwise distance between coordinates of the target conformation. N gives the number of pairs included in the biased set of n atoms. With the use of this reaction coordinate instead of the RMSD to target, removal of the rotation and translation of the center of mass at each step is avoided. A time-dependent perturbation is added to the energy function

$$V(t) = \begin{cases} \frac{A}{2}[R(t) - R_u(t)]^2 & \text{if } R(t) > R_u(t) \\ 0 & \text{if } R(t) \le R_u(t) \end{cases} \quad (2)$$

where the biasing parameter, $R_u(t)$, is updated at each step to the minimum value of $R(t)$ attained until time t. The initial value of $R_u(t)$ is obtained using the initial and target coordinates. The force constant, A, governs the rate with which the conformational transition takes place. The force constant, A, for the whole system was chosen such that the pairwise force constant, α, was 0.0004, 0.0009, 0.0013, or 0.0022 kcal/(mol Å^4). The perturbation is added to the system only when it moves away from the target. $R_u(t)$ is updated only when $V(t)$ is zero, making the pathway adiabatic.

The reaction coordinate to calculate the conformational transition pathway between CD_{down} and CD_{act} included all Lyn catalytic domain heavy atoms between residues Lys252 and Thr523 or $\sim 2.5 \times 10^6$ atom pairs. Initial and target coordinates were from the equilibrated systems for CD with ATP and Mg^{2+}. The biased MD simulations were calculated for 1.5 nsec or until the overall RMSD of heavy atoms to target structure reached a limiting value.

Trajectory analysis

The RMSD of the trajectory time points or snapshots from the target structure was used to measure completeness of the calculated pathway. The overall RMSD for all heavy atoms was calculated after superimposing the snapshots on the target structure based on all heavy atoms. For calculations of local RMSD, the superposition was based on the heavy atoms of the C-lobe. The dihedral angle time profiles were used to follow the A-loop secondary structure. The helicity was calculated for residues 413–422 of the A-loop by enumerating the backbone angles within the helical region of conformational space. (A residue is helical when its backbone dihedral angle is within $\pm 30°$ of the ideal helix values $\phi = -57°$, $\psi = -47°$ [Daggett and Levitt 1992].)

Formation and disruption of contacts along the calculated pathways were assessed from time profiles of the interatomic distances and interaction energies between two residues. The contact distance between two residues is the distance between the polar atoms of least separation. The interaction energy between two residues is equal to the nonbonded terms (electrostatic + van der Waals) for all interresidue atom pairs.

Acknowledgments

We thank Dr. Robert Geahlen and Dr. Todd Miller for useful discussions. This work was supported by NIH grant GM39478 (C.B.P.), a Purdue University reinvestment grant, and the Purdue Cancer Center (CA23568). E.O. was supported by a Purdue Research Foundation Fellowship.

References

Adams, J.A. 2003. Activation loop phosphorylation and catalysis in protein kinases: Is there functional evidence for the autoinhibitor model? *Biochemistry* **42:** 601–607.

Banavali, N. and Roux, B. 2005. The N-terminal end of the catalytic domain of Src kinase Hck is a conformational switch implicated in long-range allosteric regulation. *Structure* **13:** 1715–1723.

Barker, S., Kassel, D., Weigl, D., Huang, X., Luther, M., and Knight, W. 1995. Characterization of pp60c-Src tyrosine kinase activities using a continuous assay: Autoactivation of the enzyme is an intermolecular autophosphorylation process. *Biochemistry* **34:** 14843–14851.

Boggon, T. and Eck, M.J. 2004. Structure and regulation of Src family kinases. *Oncogene* **23:** 7918–7927.

Bolen, J.B. and Brugge, J.S. 1997. Leukocyte protein tyrosine kinases: Potential targets for drug discovery. *Annu. Rev. Immunol.* **15:** 371–404.

Breitenlechner, C., Kairies, N., Honold, K., Scheiblich, S., Koll, H., Greiter, E., Koch, S., Shafer, W., Huber, R., and Engh, R. 2005. Crystal structures of active Src kinase domain complexes. *J. Mol. Biol.* **353:** 222–231.

Brooks, B.R., Bruccoleri, R.E., Olafson, B.D., States, D.J., Swaminathan, S., and Karplus, M. 1983. CHARMM: A program for macromolecular energy minimization, and dynamics calculations. *J. Comput. Chem.* **4:** 187–217.

Bryant, Z., Pande, V., and Rokhsar, D. 2000. Mechanical unfolding of a β-hairpin using molecular dynamics. *Biophys. J.* **78:** 584–589.

Burkhardt, A., Brunswick, M., Bolen, J., and Mond, J. 1991. Anti-immunoglobulin stimulation of B lymphocytes activates Src-related tyrosine kinases. *Proc. Natl. Acad. Sci.* **88:** 7410–7414.

Capdeville, R., Buchdunger, E., Zimmermann, J., and Matter, A. 2002. Glivec (sti571, imatinib), a rationally developed, targeted anticancer drug. *Nat. Rev. Drug Discov.* **1:** 493–502.

Chan, V.W.F., Meng, F., Soriano, P., DeFranco, A.L., and Lowell, C. 1997. Characterization of the B lymphocyte populations in Lyn-deficient mice and the role of Lyn in signal initiation and downregulation. *Immunity* **7:** 69–81.

Chan, V.W.F., Lowell, C.A., and DeFranco, A.L. 1998. Defective negative regulation of antigen receptor signaling in Lyn-deficient B lymphocytes. *Curr. Biol.* **8:** 545–553.

Cowan-Jacob, S., Fendrich, G., Manley, P., Jahnke, W., Fabbro, D., Liebetanz, J., and Meyer, T. 2005. The crystal structure of a c-Src complex in an active conformation suggests possible steps in c-Src activation. *Structure* **13:** 861–871.

Daggett, V. and Levitt, M. 1992. Molecular dynamics simulations of helix denaturation. *J. Mol. Biol.* **223:** 1121–1138.

Darden, T., York, D., and Pedersen, L. 1993. Particle mesh ewald (pme): A nlog(n) method for ewald sums in large systems. *J. Chem. Phys.* **98:** 10089–10092.

Diaz, J.F., Wroblowski, B., Schlitter, J., and Engelborghs, Y. 1997. Calculation of pathways for the conformational transition between the GTP- and GDP-bound states of the Ha-ras-p21 protein: Calculations with explicit solvent simulations and comparison with calculations in vacuum. *Proteins* **28:** 434–451.

Feng, M.-H., Philippopoulos, M., MacKerell Jr., A., and Lim, C. 1996. Structural characterization of the phosphotyrosine binding region of a high-affinity SH2 domain-phosphopeptide complex by molecular dynamics simulation and chemical shift calculations. *J. Am. Chem. Soc.* **118:** 11265–11277.

Gaul, B.S., Harrison, M.L., Geahlen, R.L., Burton, R.K., and Post, C.B. 2000. Substrate recognition by the Lyn protein-tyrosine kinase: NMR structure of the immunoreceptor tyrosine-based activation motif signaling region of the B cell antigen receptor. *J. Biol. Chem.* **275:** 16174–16182.

Gibbs, C.S. and Zoller, M.J. 1991. Rational scanning mutagenesis of a protein-kinase identifies functional regions involved in catalysis and substrate interactions. *J. Biol. Chem.* **266:** 8923–8931.

Hong, J., Yankee, T., Harrison, M., and Geahlen, R. 2002. Regulation of signaling in B cells through the phosphorylation of Syk on linker region tyrosines. *J. Biol. Chem.* **277:** 31703–31714.

Hoover, W. 1985. Canonical dynamics: Equilibrium phase-space distribution. *Phys. Rev. A* **31:** 1695–1697.

Humphrey, W., Dalke, A., and Schulten, K. 1996. VMD: Visual molecular dynamics. *J. Mol. Graph.* **14:** 33–38.

Isralewitz, B., Baudry, J., Gullingsrud, J., Kosztin, D., and Schulten, K. 2001a. Steered molecular dynamics investigations of protein function. *J. Mol. Graph. Model.* **19:** 13–25.

Isralewitz, B., Gao, M., and Schulten, K. 2001b. Steered molecular dynamics and mechanical functions of proteins. *Curr. Opin. Struct. Biol.* **11:** 224–230.

Jorgensen, W. 1981. Transferable intermolecular potential functions for water, alcohols and ethers. application to liquid water. *J. Am. Chem. Soc.* **103:** 335–340.

Kamps, M. and Sefton, B.M. 1986. Neither arginine nor histidine can carry out the function of Lys295 in the ATP-binding site of p60-Src. *Mol. Cell. Biol.* **6:** 751–757.

Knighton, D.R., Zheng, J.H., Ten Eyck, L.F., Ashford, V.A., Xuong, N.H., Taylor, S.S., and Sowadski, J.M. 1991. Crystal structure of the catalytic subunit of cyclic adenosine-monophosphate dependent protein-kinase. *Science* **253:** 407–414.

Krause, D. and Van Etten, R. 2005. Tyrosine kinases as targets for cancer therapy. *N. Engl. J. Med.* **353:** 172–187.

Kwak, E.L., Sordella, R., Bell, D.W., Godin-Heymann, N., Okimoto, R.A., Brannigan, B.W., Harris, P.L., Driscoll, D.R., Fidias, P., Lynch, T.J., et al. 2005. Irreversible inhibitors of the egf receptor may circumvent acquired resistance to gefitinib. *Proc. Natl. Acad. Sci.* **102:** 7665–7670.

Lazaridis, T. and Karplus, M. 1999. Effective energy function for proteins in solution. *Proteins* **35:** 133–152.

Li, Y., Zhou, Z., and Post, C.B. 2005. Dissociation of an antiviral compound from the internal pocket of human rhinovirus 14 capsid. *Proc. Natl. Acad. Sci.* **102:** 7529–7534.

Lowell, C.A. and Soriano, P. 1996. Knockouts of Src-family kinases: Stiff bones, wimpy T cells, and bad memories. *Genes & Dev.* **10:** 1845–1857.

Lowell, C.A., Soriano, P., and Varmus, H.E. 1994. Functional overlap in the Src gene family — Inactivation of Hck and Fgr impairs natural immunity. *Genes & Dev.* **8:** 387–398.

Lutz, M., Esser, I., Flossmann-Kast, B., Vogelmann, R., Luhrs, H., Friess, H., Buchler, M., and Adler, G. 1998. Overexpression and activation of the tyrosine kinase Src in human pancreatic carcinoma. *Biochem. Biophys. Res. Commun.* **243:** 503–508.

Ma, J. and Karplus, M. 1997. Molecular switch in signal transduction: Reaction paths of the conformational changes in ras p21. *Proc. Natl. Acad. Sci.* **94:** 11905–11910.

Ma, J., Sigler, P.B., Xu, Z., and Karplus, M. 2000. A dynamic model for the allosteric mechanism of GroEL. *J. Mol. Biol.* **302:** 303–313.

MacKerell Jr., A.D., Bashford, D., Bellott, M., Dunbrack Jr., R., Evanseck, J., Field, M., Fischer, S., Gao, J., Guo, H., Ha, S., et al. 1998. All-atom empirical potential for molecular modeling and dynamics studies of proteins. *J. Phys. Chem. B* **102:** 3586–3616.

Marchi, M. and Ballone, P. 1999. Adiabatic bias molecular dynamics: A method to navigate the conformational space of complex molecular systems. *J. Chem. Phys.* **110:** 3697–3702.

McLaughlin, S. and Aderem, A. 1995. The myristoyl-electrostatic switch: A modulator of reversible protein-membrane interactions. *Trends Biochem. Sci.* **20:** 272–276.

Moarefi, I., LaFevre-Bernt, M., Sicheri, F., Huse, M., Lee, C., Kuriyan, J., and Miller, T. 1997. Activation of the Src-family tyrosine kinase Hck by SH3 domain displacement. *Nature* **385:** 650–653.

Morra, G., Hodoscek, M., and Knapp, E. 2003. Unfolding of the cold shock protein studied with biased molecular dynamics. *Proteins* **53:** 597–606.

Neria, E., Fischer, S., and Karplus, M. 1996. Simulation of activation free energies in molecular systems. *J. Chem. Phys.* **105:** 1902–1921.

Nishizumi, H., Horikawa, K., Mlinaric-Rascan, I., and Yamamoto, T. 1998. A double-edged kinase Lyn: A positive and negative regulator for antigen receptor-mediated signals. *J. Exp. Med.* **187:** 1343–1348.

Noble, M.E.M., Endicott, J.A., and Johnson, L.N. 2004. Protein kinase inhibitors: Insights into drug design from structure. *Science* **303:** 1800–1805.

Paci, E. and Karplus, M. 1999. Forced unfolding of fibronectin type 3 modules: An analysis by biased molecular dynamics simulations. *J. Mol. Biol.* **288:** 441–459.

Paci, E., Caflisch, A., Pluckthun, A., and Karplus, M. 2001. Forces and energetics of hapten-antibody dissociation: A biased molecular dynamics sudy. *J. Mol. Biol.* **314:** 589–605.

Porter, M., Schindler, T., Kuriyan, J., and Miller, W.T. 2000. Reciprocal regulation of Hck activity by phosphorylation of Tyr(527) and Tyr(416): Effect of introducing a high affinity intramolecular SH2 ligand. *J. Biol. Chem.* **275:** 2721–2726.

Rost, B. 1999. Twilight zone of protein sequence alignments. *Protein Eng.* **12:** 85–94.

Sali, A. and Blundell, T.L. 1993. Comparative protein modeling by satisfaction of spatial restraints. *J. Mol. Biol.* **234:** 779–815.

Schindler, T., Sicheri, F., Pico, A., Gazit, A., Levitzki, A., and Kuriyan, J. 1999. Crystal structure of Hck in complex with a Src family-selective tyrosine kinase inhibitor. *Mol. Cell* **3:** 639–648.

Schindler, T., Bornmann, W., Pellicana, P., Miller, W.T., Clarkson, B., and Kuriyan, J. 2000. Structural mechanism for STI-571 inhibition of Abelson tyrosine kinase. *Science* **289:** 1938–1942.

Schlitter, J., Engels, M., Kruger, P., Jacoby, E., and Wollmer, A. 1993. Targeted molecular dynamics simulation of conformational change: Application to the T-R transition in insulin. *Mol. Simul.* **10:** 291–308.

Shaffer, J. and Adams, J.A. 1999. Detection of conformational changes along the kinetic pathway of protein kinase A using a catalytic trapping technique. *Biochemistry* **38:** 12072–12079.

Sicheri, F. and Kuriyan, J. 1997. Structures of Src-family tyrosine kinases. *Curr. Opin. Struct. Biol.* **7:** 777–785.

Sicheri, F., Moarefi, I., and Kuriyan, J. 1997. Crystal structure of the Src family tyrosine kinase Hck. *Nature* **385:** 602–609.

Smith, K.G.C., Tarlinton, D.M., Doody, G.M., Hibbs, M.L., and Fearon, D.T. 1998. Inhibition of the B cell by CD22: A requirement for Lyn. *J. Exp. Med.* **187:** 807–811.

Snyder, M., Bishop, J., McGrath, J., and Levinson, A. 1985. A mutation at the ATP-binding site of pp60v-src abolishes kinase activity, transformation, and tumorigenicity. *Mol. Cell. Biol.* **5:** 1772–1779.

Süel, G., Lockless, S., Wall, M., and Ranganathan, R. 2003. Evolutionarily conserved networks of residues mediate allosteric communication in proteins. *Nat. Struct. Biol.* **10:** 59–69.

Thomas, S.M. and Brugge, J.S. 1997. Cellular functions regulated by Src family kinases. *Annu. Rev. Cell Dev. Biol.* **13:** 513–609.

Verbeek, B., Vroom, T., Adriaansen-Slot, S., Ottenhoff-Kalff, A., Geertzema, J., Hennipman, A., and Rijksen, G. 1996. c-Src protein expression is increased in human breast cancer. An immunochemical and biochemical analysis. *J. Pathol.* **180:** 383–388.

Volkman, B., Lipson, D., Wemmer, D., and Kern, D. 2001. Two-state allosteric behavior in a single-domain signaling protein. *Science* **291:** 2429–2433.

Williams, J., Weijland, A., Gonfloni, S., Thompson, A., Courtneidge, S., Superti-Furga, G., and Wierenga, R. 1997. The 2.35 crystal structure of the inactivated form of chicken Src: A dynamic molecule with multiple regulatory interactions. *J. Mol. Biol.* **274:** 757–775.

Xu, W., Harrison, S., and Eck, M.J. 1997. Three-dimensional structure of the tyrosine kinase c-Src. *Nature* **385:** 595–602.

Xu, W., Doshi, A., Lei, M., Eck, M.J., and Harrison, S.C. 1999. Crystal structure of c-Src reveals features of its autoinhibitory mechanism. *Mol. Cell* **3:** 629–638.

Yamaguchi, H. and Hendrickson, W.A. 1996. Structural basis for activation of human lymphocyte kinase Lck upon tyrosine phosphorylation. *Nature* **384:** 484–489.

Yamanashi, Y., Kakiuchi, T., Mizuguchi, J., Yamamoto, T., and Toyoshima, K. 1991. Association of B cell antigen receptor with protein tyrosine kinase Lyn. *Science* **251:** 192–194.

Young, M.A., Gonfloni, S., Superti-Furga, G., Roux, B., and Kuriyan, J. 2001. Dynamic coupling between the SH2 and SH3 domains of c-Src and Hck underlies their inactivation by C-terminal tyrosine phosphorylation. *Cell* **105:** 115–126.

Zheng, W., Brooks, B.R., Doniach, S., and Thirumalai, D. 2005. Network of dynamically important residues in the open/closed transition in polymerases is strongly conserved. *Structure* **13:** 565–577.

Zhu, X., Kim, J., Newcomb, J., Rose, P., Stover, D., Toledo, L., Zhao, H., and Morgenstern, K. 1999. Structural analysis of the lymphocyte-specific kinase Lck in complex with non-selective and Src family selective kinase inhibitors. *Structure* **7:** 651–661.